Reprinted from

SURFACE & COATINGS TECHNOLOGY

Surface and Coatings Technology 115 (1999) 249–255

Surface hardening of low-alloy 15CrNi6 steel by CO_2 laser beam

A.I. Katsamas *, G.N. Haidemenopoulos

Department of Mechanical & Industrial Engineering, University of Thessaly, 383 34 Volos, Greece

Received 15 February 1999; accepted 5 May 1999

ELSEVIER

ELSEVIER

Surface and Coatings Technology 115 (1999) 249–255

SURFACE & COATINGS TECHNOLOGY

www.elsevier.nl/locate/surfcoat

Surface hardening of low-alloy 15CrNi6 steel by CO_2 laser beam

A.I. Katsamas *, G.N. Haidemenopoulos

Department of Mechanical & Industrial Engineering, University of Thessaly, 383 34 Volos, Greece

Received 15 February 1999; accepted 5 May 1999

Abstract

The study investigates laser transformation hardening in the low-alloy 15CrNi6 case-hardening steel. The effect of process parameters such as beam power, beam diameter and travel speed on microstructure, case depth and hardness was examined. In addition, the effect of surface preparation was also investigated. For this purpose, all specimens were initially sandblasted, and some were additionally coated with graphite in order to enhance surface absorptivity. In most cases, a heat affected zone (HAZ) formed below the surface. This consisted of two discrete areas, a surface layer and a transition area between this surface layer and the base metal. The microstructure of the surface layer was found to consist of lath martensite, while carburization was found for certain process conditions in the graphite-coated specimens. The transition area consisted of a dispersion of fine carbides in a ferrite matrix. A substantial increase in surface hardness was achieved, by a factor of 2.5 times the base metal hardness. Depths of the HAZ up to approximately 0.6 mm were obtained, without surface melting. The additional use of graphite coating enhanced, in most cases, the coupling of laser-beam to the surface resulting in greater HAZ depths.

Keywords: Carburizing; Laser transformation hardening; Microstructure analysis; 15CrNi6 low-alloy steel

1. Introduction

Laser transformation hardening has become a well established technique for heat treating steel surfaces, competing against the more widely used flame and induction hardening methods. The process presents considerable advantages over these alternative methods — the most significant are the high degree of controllability and automation, low part distortion and capability of very selective and precise treatment [1].

The process uses the heat generated by the impingement of a laser beam on the surface of the material to austenitize it. The austenitized layers are subsequently transformed to martensite due to very rapid conduction of heat into the cold interior of the workpiece. This effect is known as self-quenching and the cooling rates obtained are usually high enough to allow martensite formation, even in steels which have very low hardenability [2]. In addition, the hardened microstructure obtained is usually finer than that from conventional hardening techniques, leading to increased hardness and consequently to increased wear and fatigue resistance [2,3].

The effect of the process on the hardened depth depends strongly on the process parameters used, as well as on the thermo–physical properties of the material [4]. The major process parameters involved are beam power and size, relative travel speed between the laser beam and the workpiece, and the absorptivity of the surface to laser radiation. The infrared radiation produced by CO_2 lasers, which are usually employed in transformation hardening, is absorbed in very small fractions by steel surfaces. In order to increase absorptivity and make more efficient use of the available laser power, the surface is often pre-coated with graphite, manganese phosphate or other absorbing coatings [1,2].

The present work is an experimental study of laser transformation hardening of 15CrNi6 low-alloy steel. The effects of process parameters and surface preparation on the resulting microstructure and properties of the steel were investigated. This study is a part of a series of researches on surface transformation hardening of plain carbon and low-alloy steels (other parts have been published elsewhere [5,6]). Investigation of the present material served as a first step towards laser

* Corresponding author. Tel.: +30-421-74061; fax: +30-421-69787.
E-mail address: akatsam@uth.gr (A.I. Katsamas)

0257-8972/99/$ – see front matter
PII: S0257-8972(99)00246-7

carburizing, which is currently being undertaken by the authors.

2. Experimental procedure

The material used in this study was 15CrNi6 steel which belongs to the high quality, alloyed steels group. It is a case hardening steel mainly used for cog-wheels, chain wheels and other parts in the automotive industry [7]. The composition of the material was obtained by chemical analysis (SPECTROLAB M5) and is presented in Table 1.

For the experiments, 6 mm thick discs were cut from 100 mm diameter round bars of the material. All the discs were sandblasted (S-specimens) in order to increase the absorptivity of their surfaces to the laser beam radiation. After sandblasting, some of the discs were also coated with graphite spray (GRAPHIT 33) in an effort to increase the absorptivity of the steel surface (SG-specimens) even further.

The experiments were carried out using a CO_2 continuous wave laser (LASER ECOSSE) capable of providing a maximum output power of 3 kW. The laser beam had a circular cross-section and the power distribution within it followed the TEM^{*}_{01} mode, also known as a 'doughnut' mode due to its shape. The workpieces were appropriately held on a CNC-table which had the ability to move within a certain range of speeds. During the process, the laser beam was kept stationary while the table was translated with a specified travel speed with respect to the beam.

A wide variety of process conditions (beam power, beam diameter and travel speed) were used in the experiments (Table 2), producing single tracks over the surface of the discs. N_2 at a pressure of 5 bar was used as protective gas against oxidation.

Specimens for metallographic examination by optical microscopy were cut perpendicular to the beam direction, while some of the specimens were taper-sectioned at a random angle from the surface. All the specimens were embedded into resin, ground and polished. Etching was performed using Nital 2% or Villela's (100 ml ethanol, 5 ml HCl, 1 g picric acid [8]) reagents. Microhardness was measured as a function of depth below the surface for all the laser treated specimens using a load of 0.2 kg.

Table 1
Chemical composition (wt.%) of 15CrNi6 steel

C	Si	Mn	P	S	Cr	Ni	Fe
0.15	0.37	0.53	0.014	0.028	1.65	1.51	bal.

Table 2
Process conditions and surface preparation used in the experiments on steel 15CrNi6

Beam power (kW)	Beam diameter (mm)	Travel speed (m/min)	Surface preparation
1.5	2.75	3–10.5	sandblasted
	4.15	4.5–9	
	6	4.5–7.5	
3	4.15	7.5–13.15	
	6	7.5–13.15	
	7.25	7.5–10.5	
1.5	2.75	3–10.5	sandblasted plus graphite coated
	4.15	4.5–9	
	6	1.5–7.5	
3	4.15	6–18	
	6	4.5–13.5	
	7.25	1.5–7.5	

3. Results and discussion

3.1. Starting microstructure

The starting microstructure of steel 15CrNi6 (Figs. 1 and 2) consisted of 'blocky' proeutectoid ferrite of allotriomorphic morphology [9], fine pearlite and grey etching regions which appear to be sheaves of upper bainite. The microstructure is also shown in the optical micrograph of Fig. 2.

The evolution of the starting microstructure on heating, as well as the intercritical temperature range of the steel, were determined using the computational alloy thermodynamics software Thermo–Calc [10]. A system with the chemical composition of Table 1 was defined and, of all the possible phases that can form in this system, the following were chosen as the most probable of being thermodynamically stable, to be taken account of in the calculation: bcc (ferrite), fcc (austenite), cementite (M_3C), $M_{23}C_6$, M_7C_3, M_3C_2 and M_5C_2. M in these

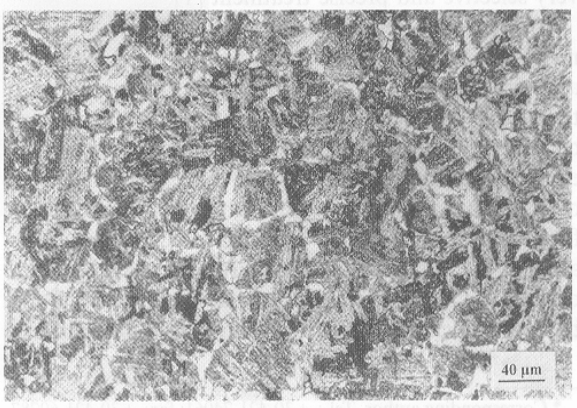

Fig. 1. Starting microstructure of steel 15CrNi6.

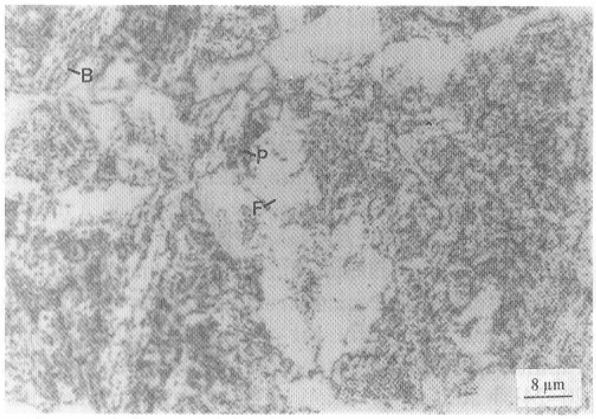

Fig. 2. Proeutectoid ferrite (F), pearlite (P) and upper bainite (B) in the starting microstructure.

carbides could be any of the metallic elements of the alloy (Fe, Cr, Mn or Ni). The thermodynamically stable phases and the determination of the critical temperatures A_{e1} and A_{e3} are summarised in Fig. 3(a).

Note that the initially stable phases are ferrite and the M_7C_3 carbide. Fig. 3(b) depicts the weight fraction

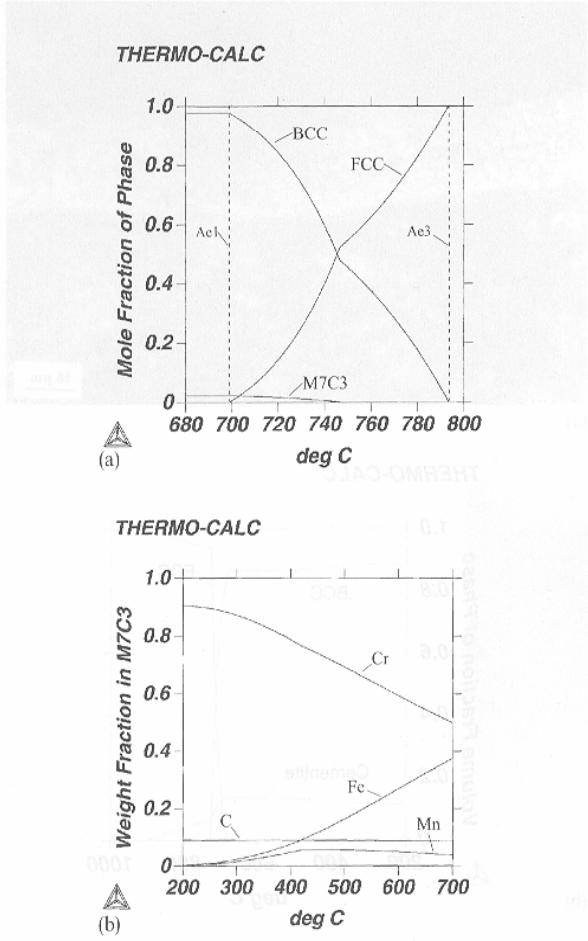

Fig. 3. (a) mole fraction of the equilibrium phases of the steel, and (b) weight fraction of alloy elements in the M_7C_3 carbide, as a function of temperature.

of the alloy elements in this carbide phase as a function of temperature. At relatively high temperatures (400 – 700 °C) the carbide contains mainly Cr but also substantial amounts of Fe and Mn. At lower temperatures, and down to room temperature, the metallic constituent of the carbide is exclusively Cr.

Cementite, despite the fact that it has been accounted for in the calculation, does not appear to be the equilibrium carbide phase. This supports the idea that the pearlite observed could be an alloy pearlite composed of ferrite and M_7C_3. Honeycombe [11] comments on alloy pearlite claiming that the change in carbide phase does not necessarily alter the basic pearlitic morphology, and that its existence has been reported in medium and highly-alloyed steels. However, although cementite is not the equilibrium carbide in many alloy steels, it is kinetically favoured because its formation can occur by a mechanism which does not necessitate the long-range diffusion of substitutional solutes [12]. Thus, the observed carbides in the starting microstructure of the steel are more likely to consist of cementite (M_3C), rather than the equilibrium M_7C_3 carbide.

The existence of sheaves of upper bainite in the microstructure of steel 15CrNi6, which consist of ferrite laths and cementite precipitates between those laths, could be attributed to the relatively high temperature for the start of the bainitic transformation (B_s) in this particular steel. The B_s temperature, estimated using an empirical equation proposed by Steven and Haynes [13], is 570 °C. Thus, during heat treatment of the steel it is quite probable to have the initiation of the bainitic transformation, which proceeds to some extent, leading to the formation of upper bainite.

Regarding the determination of the critical equilibrium temperatures, it can be seen from Fig. 3(a) that the A_{e1} temperature, i.e. the temperature at which austenite starts to form, is 699°C, while the Cr_7C_3 carbide completely dissolves at 747°C. Finally, the A_{e3} temperature, corresponding to full austenitization, was determined to be 794°C.

Heat treatment with laser beams, however, induces a thermal cycle to the material which is far from equilibrium due to the very high heating rates obtained. Heating rates in the order of 10^4 K/s, and even greater, have been reported accompanied by very short austenitizing times [14]. It is well established that non-equilibrium heating of steels, leads to a shift of the critical temperatures to higher values [15]. Studies have been reported where the A_{c3} temperature (full austenitizing temperature on heating) was more than 200°C greater than A_{e3} in rapidly heated low and medium carbon steels [16–18]. Nevertheless, the sequence of transformations on heating, and the phases which participate in them, does not change, following from that point of view those predicted by equilibrium.

3.2. Microstructural modifications due to laser-treatment

Fig. 4 shows the transverse section of one of the laser-treated specimens. Three distinct areas can be seen. The first one is more lightly etched and forms a very shallow layer on the surface of the material. Below this there exists a more darkly etched region which extends at greater depths below the surface. These two regions form a zone on the surface, which has clearly undergone a series of phase transformations and is called a 'heat affected zone' here (HAZ). Finally, the grey area at the bottom is the part of the material which remained unaffected by the process. In some specimens the more lightly etched top surface area had not formed.

The microstructure in the top surface area of the sandblasted (S) specimens was found to consist of lath martensite, Fig. 5, which represents a taper-section of the surface at a random angle. This microstructure is an indication that the thermal cycle in this zone, despite the very rapid heating and small austenitizing times, fully austenitizes the surface region.

The lightly etched top surface area was also present in the graphite coated (SG) specimens. However, in some specimens significant differences in the microstructure of this layer were observed which indicated a possible carburizing of the steel surface. The microstructure shown in Fig. 6(a) is characteristic of a carburized steel [19]. The carbide phase outlines prior austenite grains, while martensite plates are observed in a matrix of retained austenite. At the interface with the darkly etched region martensitic plates have formed, a typical feature of carburized microstructures. Laser carburizing of iron and steels, by pre-coating the surface with graphite, has also been reported by other investigators [20–24], leading to a variety of microstructures depending on process parameters and thickness of the coating. The nature of the carbide phase was determined by calculating the volume fraction of stable phases as a function of temperature for various carbon contents of the steel in the range of 0.15 wt.% (initial content) to 2 wt.%. The calculation was carried out using the Thermo–Calc software and Fig. 6(b) shows a characteristic volume fraction against temperature diagram for a

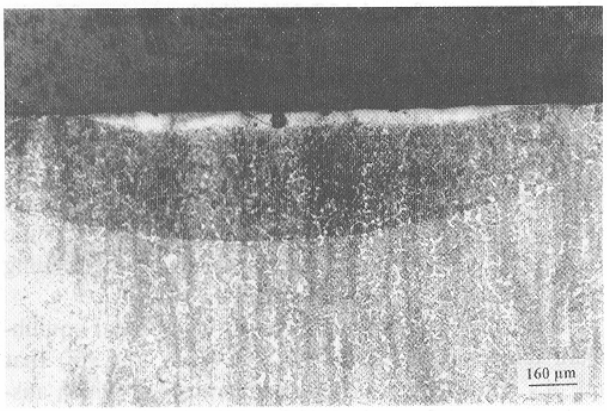

Fig. 4. Transverse section of a laser-treated specimen showing the HAZ and the base metal below the surface.

Fig. 5. Taper-section of a sandblasted specimen showing a lath martensitic microstructure in the surface layer.

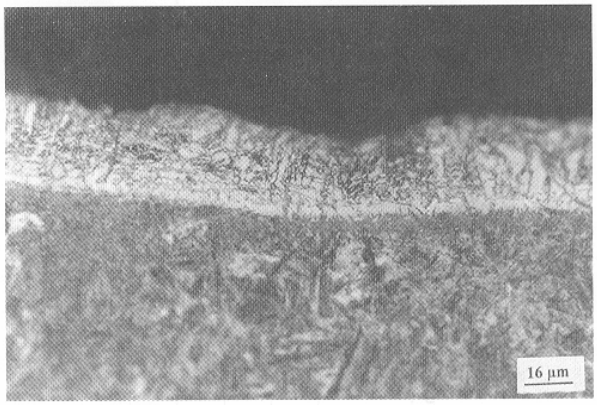

(a)

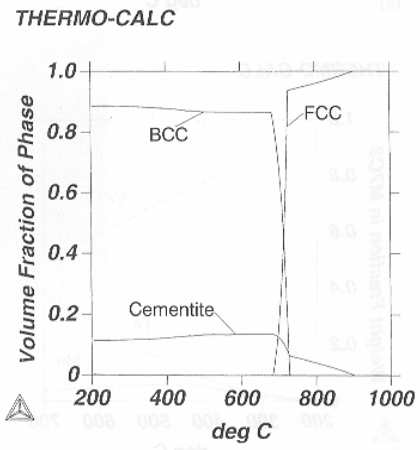

(b)

Fig. 6. (a) The carburized surface (lightly etched layer) of a sandblasted and graphite coated specimen, shown here in transverse section. (b) Calculated volume fractions of the stable phases in carburized 15CrNi6 steel (carbon content 1 wt.%) as a function of temperature.

carbon content of 1 wt.%. The major stable carbide phase is cementite, reaching a volume fraction of 10%, approximately the same fraction of carbide observed in the microscope. Cementite is by far the dominant carbide throughout the calculated range of carbon contents, indicating that the observed carbide is indeed of this kind.

The darkly etched region of the HAZ (Fig. 4), formed in both the S- and in the SG-specimens and is clearly a transition area between the martensitic (or carburized) layer and the base metal. Fig. 7 shows the interface between the transition region and the base metal. Although no clear border exists, the transition area possesses a finer microstructure than the base metal.

The microstructure of the transition area consists of a dispersion of fine carbides, in addition to the proeutectoid ferrite grains which were present in the starting microstructure. It is evident that the thermal cycle was inadequate to austenitize this area, but was enough to cause a tempering of the pre-existing bainitic microstructure. During tempering of the bainite, cementite tends to be replaced by the corresponding equilibrium alloy carbide [12], which in this case is the M_7C_3 (Fig. 3(a)). Such behaviour is known to take place in low-alloy martensitic and bainitic steels and leads to secondary hardening. If the tempering continues for longer times, coarsening of the carbides leads to a decrease in hardness.

3.3. Effect of process parameters on the HAZ depth

3.3.1. Sandblasted (S) specimens

The maximum HAZ depth obtained without melting the surface was approximately 0.28 mm. A HAZ up to 0.4 mm below the surface was achieved but was accompanied by severe melting of the surface to a depth of about 0.17 mm, which is usually undesirable in the process. It should be noted that the specimens irradiated with the largest beam diameters (6 mm with 1.5 kW power and 7.25 mm with 3 kW power) were not affected by the process, i.e. no microstructural change of any sort was observed in the range of travel speeds employed.

Fig. 8 depicts the depth of the HAZ as a function of process parameters for the S-specimens. The use of high power and/or small beam diameter leads to increased HAZ depths, associated with the increased power density (i.e. power per unit surface) impinging on the material. The same is also valid when the travel speed is decreased, due to the increased interaction time between the laser beam and the surface of the material. Both those effects are well established in literature.

3.3.2. Sandblasted and graphite coated (SG) specimens

The addition of a graphite coating on the already sandblasted surface led, in general, to the formation of HAZ which extended at greater depths below the surface. The maximum depth achieved without surface melting was approximately 0.59 mm. The greatest HAZ depth measured was approximately 0.86 mm below the surface, but it was accompanied by surface melting down to 0.06 mm.

The observations made in the previous section, regarding the influence of process parameters on the HAZ depth, hold also for the SG-specimens. Fig. 9 summarises the effect of process parameters on HAZ depth. The results obtained with the 1.5 kW beam and using the 2.75 mm and 4.15 mm beam diameters were quite close, so they are represented by the same curve in the diagram.

It can be seen that in the case of the SG-specimens, laser power plays a dominant role since the HAZ depths obtained with the 3 kW beam are greater than those obtained with the 1.5 kW beam, even when using a relatively large beam diameter (7.25 mm). This behaviour was not observed in the S-specimens (Fig. 8), where beam diameter seems to have an equally important effect on the HAZ depth. For example, the use of the 1.5 kW beam with a 2.75 mm diameter leads to greater HAZ

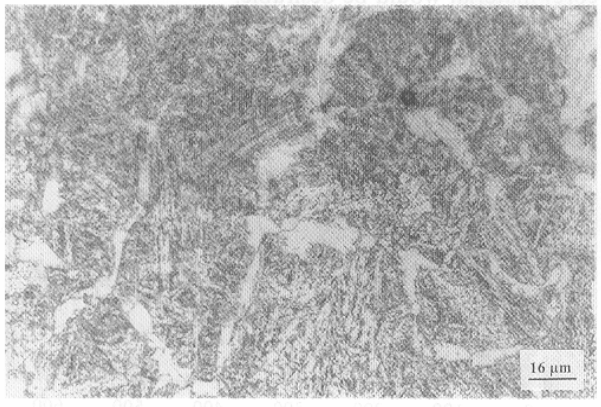

Fig. 7. Transition area (top half) and base metal (bottom half). Note the refined microstructure of the transition area consisting of tempered bainite.

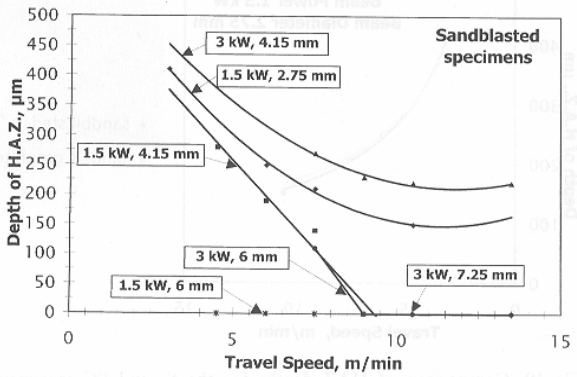

Fig. 8. Depth of the HAZ as a function of travel speed and beam diameter for the sandblasted specimens.

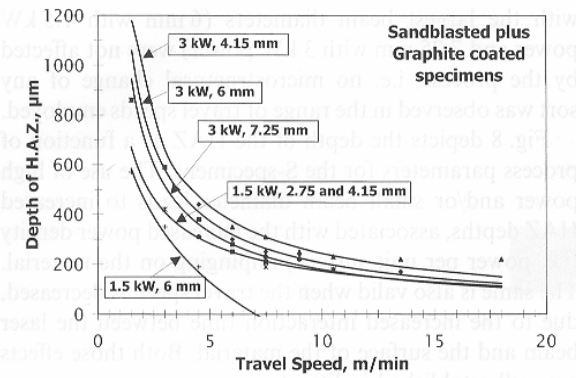

Fig. 9. Depth of the HAZ as a function of travel speed and beam diameter for the sandblasted plus graphite coated specimens.

depths than those obtained with the 3 kW and 6 mm beam. The increased significance of laser power in the SG-specimens is attributed to their higher surface absorptivity, which leads to more efficient coupling of the impinging radiation.

3.3.3. Effect of graphite coating

In general, the SG-specimens presented higher depths of HAZ than the S-specimens. This is attributed to the enhancement of surface absorptivity caused by the addition of the graphite coating.

A behaviour different from that was only observed in the specimens treated with a beam power of 1.5 kW and a 2.75 mm diameter beam (Fig. 10) where no significant differences between the S- and SG-specimens were observed. This could be attributed to the behaviour of the graphite coating during treatment with the smaller beam diameter. Applying the graphite coating by hand does not ensure homogeneity. Keeping that in mind, it should be noted that as the beam becomes smaller it is influenced to a greater extent by such inhomogeneities, rather than in the case of a larger beam where inhomogeneities tend to compensate due to the larger area covered by the beam. Another possible explanation is that a small beam diameter introduces a higher power density on the surface, which in turn leads to the development of higher temperatures. This could force the graphite coating to evaporate, or even violently eject from the surface, before it even starts to interact with the beam thus lowering surface absorptivity.

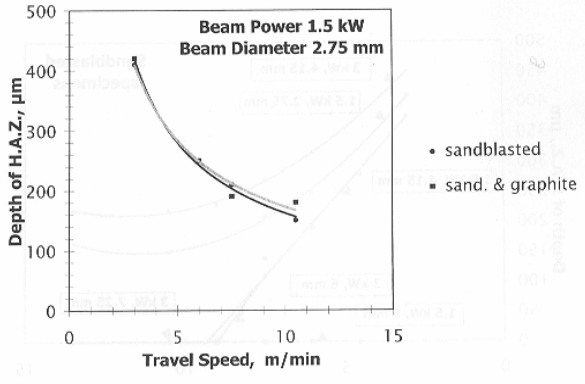

Fig. 10. Comparison of HAZ depths for the S- and SG-specimens treated under the conditions shown in the diagram. No significant differences were found, despite the additional use of graphite coating.

4. Microhardness measurements

The microhardness of steel 15CrNi6 was initially measured at 200 $HV_{0.2}$, a value consistent with the microstructure observed before laser irradiation. After laser treatment, a significant enhancement of the specimens' surface hardness was obtained. For those specimens with a fully martensitic zone on the surface, the mean value of microhardness reached 500 $HV_{0.2}$, in agreement with the expected microhardness of an as-quenched steel, containing 0.15 wt.% carbon [25].

The existence of two areas within the HAZ of the irradiated specimens is reflected in the corresponding microhardness profiles, Fig. 11. The shallow martensitic layer on the surface had a microhardness approaching 500 $HV_{0.2}$. A gradual decrease of the microhardness occurred within the transition region, which nevertheless remained higher than the base metal. This is attributed to the secondary hardening effect and is in agreement with the microstructural observations in that region. Finally, the base metal microhardness was unaltered at 200 $HV_{0.2}$.

The lack of any fully martensitic zone in some specimens resulted in microhardness profiles such as the one shown in Fig. 12, which is similar to the one in Fig. 11 if the martensitic zone is omitted. Despite the fact that a martensitic zone is not fully formed, the enhancement of surface microhardness is still substantial. Such a hardness distribution could be useful in applications where a gradually softer (from surface to core) material would be desirable.

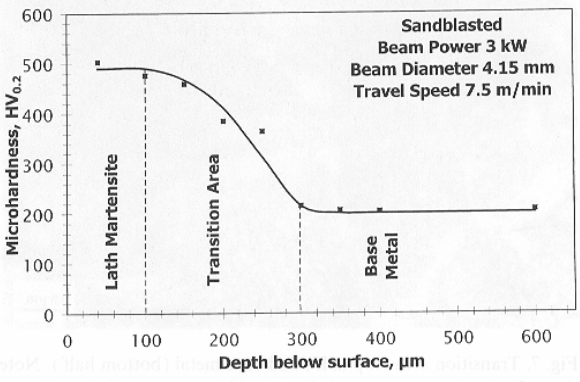

Fig. 11. Microhardness profile of a laser-treated specimen.

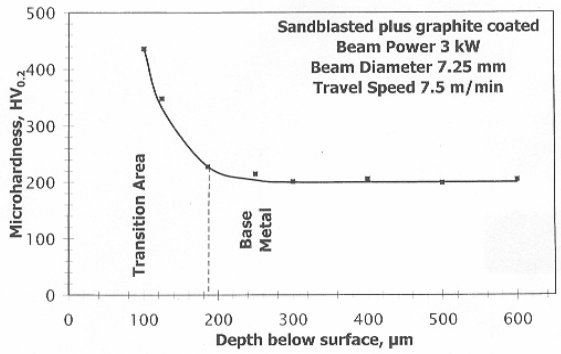

Fig. 12. Profiles such as the one shown here were observed in specimens lacking the fully austenitized surface layer.

5. Conclusions

The experimental investigation of laser surface hardening of the 15CrNi6 low-alloy steel, has led to the following remarks:

1. the process causes a significant hardening effect on the surface of the material, despite the fact that this steel has a relatively low carbon content. The microhardness of the surface has increased by a factor of about 2.5 times the initial (prior to laser treatment) microhardness of the material;
2. hardening is a result of the formation of a heat affected zone (HAZ) on the surface which in most cases comprises of two discrete regions — one which is fully austenitized and another which is a transition area between the austenitized region and the base metal;
3. the microstructure of the fully austenitized layer depends on whether the specimen was coated with graphite or not, and consisted of lath martensite in the sandblasted specimens, while in some of the sandblasted plus graphite coated specimens this layer had been carburized and consisted of a cementite network, martensite plates and retained austenite;
4. a tempering of the initial bainitic microstructure of the steel took place inside the transition area resulting in a dispersion of fine equilibrium M_7C_3 carbide, accompanied by a secondary hardening effect;
5. HAZ depths up to about 0.6 mm were achieved without melting the surface. The HAZ depth depends strongly on process parameters, and it increases by either increasing the beam power or by decreasing the travel speed or the beam diameter;
6. the addition of graphite coating on the surface prior to the treatment resulted, in general, in greater HAZ depths by enhancing surface absorptivity.

Acknowledgements

The authors would like to thank the Laser Innovation Centre of the Foundation for Research and Technology Hellas (LIC/FORTH) for kindly allowing the use of the 3 kW CO_2 laser. This work has been partly supported by the General Secretarial of Research and Technology through the EPET II/170 'LaserMat' project.

References

[1] W.M. Steen, Laser Material Processing, 1st edition, Springer-Verlag, London, 1996.
[2] Heat Treating, A.S.M. Handbook, 9th edition. 4 A.S.M. International, Materials Park, Ohio, 1998.
[3] G. Stahli, Tribol. Intern. (April, 1981) 101–106.
[4] H.R. Shercliff, M.F. Ashby, Metall. Trans. A 22A (1991) 2459–2466.
[5] A.I. Katsamas, A.D. Zervaki, G.N. Haidemenopoulos, Steel Research 68 (3) (1997) 119–124.
[6] A.I. Katsamas, G.N. Haidemenopoulos, J. Balk. Trib. Assoc. 4 (3) (1998) 129–140.
[7] Verlag: Stahlschlussel, 1st edition, Marbach, 1986.
[8] G.F. Vander Voort, Metallography Principles and Practice, 1st edition, McGraw-Hill, London, 1984.
[9] D.A. Porter, K.E. Easterling, Phase Transformations in Metals and Alloys, 2nd edition, Chapman and Hall, London, 1992.
[10] B. Sundman, B. Jansson, J.O- Anderson, CALPHAD 9 (1985) 153.
[11] R.W.K. Honeycombe, Steels Microstructure and Properties, 1st edition, A.S.M. International, Materials Park, Ohio, 1981.
[12] H.K.D.H. Bhadeshia, Bainite in Steels, 1st edition, The Institute of Materials, London, 1992.
[13] W. Steven, A.J. Haynes, J. Iron Steel Inst. 183 (1956) 349–359.
[14] J.R. Bradley, S. Kim, Metall. Trans. A 19A (1988) 2013–2025.
[15] D. Shuocker, Handbook of the Eurolaser Academy, 1st edition. II Chapman and Hall, London, 1998.
[16] K.J. Albutt, S. Garber, J.I.S.I. 204 (1966) 1217–1222.
[17] S.-J. Na, Y.-S. Yang, Surf. Coat. Tech. 34 (1988) 319–330.
[18] A. Jacot, M. Rappaz, Acta. Mater. 45 (2) (1997) 575–585.
[19] Metallography and Microstructure, A.S.M. Handbook, 9th edition. 9 A.S.M. International, Materials Park, Ohio, 1998.
[20] A. Walker, H.M. Flower, D.R.F. West, J. Mater. Sci. 20 (1985) 989–995.
[21] P. Canova, E. Ramous, J. Mater. Sci. 21 (1986) 2143–2146.
[22] B. Grunenwald, E. Bischoff, J. Shen, F. Dausinger, Mater. Sci. Tech. 8 (1992) 637–643.
[23] M. Tayal, K. Mukherjee, Scr. Metall. Mater. 29 (1993) 1279–1284.
[24] M. Tayal, K. Mukherjee, Mater. Sci. Eng. A 174 (1994) 231–236.
[25] G. Krauss, Steels Heat Treatment and Processing Principles, 2nd edition, A.S.M. International, Materials Park, Ohio, 1990.